NaCl precleaning of microfiltration membranes fouled with oil-in-water emulsions: Impact on fouling dislodgment

C. Rouquié, Anthony Szymczyk, M. Rabiller-Baudry, H. Roberge, P. Abellan, Alain Riaublanc, M. Frappart, S. Álvarez-Blanco, Estelle Couallier

NaCl precleaning of microfiltration membranes fouled with oil-in-water emulsions: impact on fouling dislodgment

C. Rouquié[1,2,3], A. Szymczyk[1], M. Rabiller-Baudry[1], H. Roberge[2,4], P. Abellan[4], A. Riaublanc[3], M. Frappart[2], S. Álvarez-Blanco[5] , E. Couallier[2*]

[1] Univ Rennes, CNRS, ISCR (Institut des Sciences Chimiques de Rennes) – UMR 6226, F-35000 Rennes, France

[2]CNRS, GEPEA, Université de Nantes, 37 Boulevard de l'université, BP 406, 44602 Saint-Nazaire cedex, France

[3]INRA, BIA, Rue de la Géraudière, BP 71627, 44 316 Nantes Cedex 3, France

[4]CNRS, Institut des Matériaux Jean Rouxel (IMN), Université de Nantes, CNRS, 2 rue de la Houssinière, 44322 Nantes cedex 3, France

[5]Research Institute for Industrial, Radiophysical and Environmental Safety (ISIRYM), Universitat Politècnica de València, Camino de Ver s/n, 46022 Valencia, Spain

*Corresponding author: estelle.couallier@univ-nantes.fr

https://doi.org/10.1016/j.seppur.2021.120353

Abstract

Despite the growing interest in membrane filtration for biorefining of microalgae, few works have dealt with membrane regeneration after fouling by such specific vegetable products. The current procedure still requires large volumes of cleaning solutions, which leads to additional energy and water consumption with a substantial environmental impact. NaCl solutions have already been used in precleaning steps to enhance the cleaning of ultrafiltration membranes fouled by whey proteins. The aim of this work was to test this innovative procedure on membranes fouled by a representative emulsion of microalgae lipid extracts and to gain insight into how salt promotes changes in fouling organization. Polyethersulfone (PES)-based membranes with an average pore diameter of 0.1 µm were fouled by the emulsion, and then cleaned in several steps: water precleaning, NaCl precleaning, detergent cleaning and sodium hypochlorite polishing. Two salt concentrations (5 and 7.5 mM NaCl) and 2 temperatures (37.5 °C and 50 °C) were considered and compared to control experiments. The cleaning efficiency of NaCl solutions was evaluated based on the hydraulic cleaning efficiency (HCE). The 5 mM NaCl solution at 50 °C led to the best precleaning performance with an HCE of 80%. The subsequent cleaning step with detergent U115 removed the remaining fouling and achieved 100% HCE without the need for a NaClO-NaOH polishing step. The impact of salt on membrane fouling was then investigated by characterizing the surface of the (i) pristine (ii) fouled and (iii) precleaned membranes

with NaCl. Fouling was shown to occur on the surface of the membranes as well as in their porous structure, and to be irregularly organized in regions containing greater or lesser amounts of lipids. The use of NaCl significantly reduced internal fouling by moving lipids from the inside of the pores to the outer surface, thus facilitating the detergent cleaning step. This work contributes to the development of cost-effective and environmentally friendly cleaning procedures for separation processes used in many fields among which microalgae biorefinery.

Highlights:

- NaCl precleaning was used to help remove lipid fouling from PES membranes.
- The optimal precleaning conditions were 5 mM NaCl, 50°C and led to 80% HCE.
- SEM-EDX, ATR-FTIR, AFM and electrokinetic analyses were performed.
- Internal fouling and surface fouling were both impacted by NaCl precleaning.
- NaCl precleaning followed by detergent cleaning led to 100% HCE.

Keywords: lipid fouling, NaCl precleaning, polyethersulfone microfiltration membrane, SEM-EDX, electrokinetic measurements

1 Introduction

The recovery of high-added value compounds from microalgae biomass is gaining more interest due to their useful applications in various industrial fields: lipids for biofuels, proteins for feedstock, polysaccharides as viscosifiers, lubricants or flocculants for industrial applications, polyunsaturated fatty acids as nutritional supplements, carotenoids as natural food colorants, tanning aid or food supplements, glycerol for skin moisture, etc [1]. However, one of the main challenges in expanding the use of microalgae remains the development of cost-effective processes for the extraction and purification of these valuable compounds. In this regard, membrane filtration appears to be a promising separation technology, thanks to its well-known advantages (low energy consumption, low temperature, no solvent use, no phase change and easy handling) [2]. Several research works have already highlighted the interest of membrane technologies for bioactive compounds recovery from algal-based suspensions [3–9] among which lipids by micro- and ultrafiltration for biofuel production. However, the fractionation of algal products by membrane technologies is still not widespread due to several technological and scientific bottlenecks [8,9]. An ideal membrane processing of microalgae metabolites would allow the permeation of the hydrophilic protein and carbohydrate-rich fractions,

while lipids would be retained by the membrane. This has been partially achieved but yields for protein recovery are still low, with rejection rates for hydrophilic compounds being higher than expected [3,7]. The membrane fouling has led to insufficient efficiency of the separation process, thus strategies to control fouling during filtration of disrupted microalgae are needed. Consideration must be given to suspension pretreatment, selection of appropriate membrane material, *in situ* fouling prevention tools (turbulence promoters, critical flux) and post-treatment strategies (membrane cleaning). This paper focuses on this important question of membrane cleaning to overcome the fouling by microalgae extracts.

Membrane cleaning is a key step of the filtration process. The aims are the recovery of at least 90% of the reference water flux), the removal of adsorbed fouling, and the elimination of potential alive microorganisms (not considered in the present work)to ensure long-term stability of the membrane performance (flux, rejection) [10,11]. The main steps are (i) physical cleaning that may consist of deionized water rinsing, backwashing or ultrasonic vibrations, to remove weakly attached membrane fouling, commonly known as reversible fouling and (ii) chemical or enzymatic cleaning, with a cascade of formulated detergents, with deionized water inter-rinsing, to remove the remaining part of fouling that is tightly attached on the membrane surface and/or in the membrane pores [11–13]. Alkaline detergents are efficient towards organic matter deposited on polymer membranes. Generally, they contain alkali, surfactants, chelating agents. According to several authors, cleaning with acid solutions does not seem to be efficient with algal products [13,14]. (iii) Oxidants, such as sodium hypochlorite (NaClO) are usually used in Cleaning-in-Place (CIP) operations, after an alkaline step, for fouling removal completion (polishing) and disinfection. So far, sodium hypochlorite solutions have been used mainly for the chemical cleaning of ultra and microfiltration polymer membranes fouled by algae-based products. [12–16]. However, NaClO cleaning has two main drawbacks: 1) its reaction with organic precursors from algae fouling results in the formation of many toxic and carcinogenic halogenated by-products [12,15]; 2) NaClO leads to membrane degradation (e.g. loss of hydrophilic additives such as PVP or surface morphology modification) [17]. It is worth mentioning that studies reported in the literature [12–16] dealt with full cell harvesting and, to the best of our knowledge, no work has reported an in-depth investigation of the cleaning of membranes fouled by disrupted microalgae, which represents a substantial challenge in the field.

Most cleaning procedures require large volumes of water and chemical reagents, resulting in significant cleaning and effluent treatment costs. Several authors have investigated the possibility of using salt solutions for membrane regeneration in other fields, owing to their environmental friendliness and low

cost [18]. Among the various salts considered, cleaning by NaCl has proven its efficiency on different types of fouling such as protein-like substances (BSA, enzymes, whey model solutions [19–21]), humic acids [18,22], polysaccharides (alginate and pectin) [10], sodium alginate [23] and natural organic matter from river water [10]. Since these previous studies, NaCl precleaning could be an interesting pretreatment or alternative to currently used chemical reagents for microalgae-based fouling. The aim of this work was therefore to evaluate the efficiency of NaCl precleaning for the regeneration of membranes fouled with biomolecules released in water after cell disruption.

This paper mainly focuses on the cleaning of membranes fouled by lipids, which are among the most valuable products from microalgae. A simplified microemulsion was considered to simulate a concentrated extract of microalgae grown in starving conditions to produce lipids for biofuels [24,3]: it contains triglycerides stabilized by polar lipids dispersed as droplets with diameters between 0.05 and 2µm.

The operating parameters (crossflow velocity, transmembrane pressure) directly impact the oil fouling and the filtration performances (flux and retention). [25][26][27]. The permeation of the oil droplets even can occur if the transmembrane pressure overcomes the capillary entry pressure [28,29].

Despite the large number of studies with different ultra and microfiltration membranes, there is little agreement in the mechanisms of membrane fouling by emulsified oil and the structure of the resulting fouling layer. In situ investigation at a local scale can offer highly valuable insights into the fouling process [30], governed by short-range interactions between the oil, the membrane, the surfactants and the salts. New methods are being developed to describe the membrane fouling with online analytical methods [31–34], and Tanudjaja et al [32][35] showed that the behavior of oil droplets is far from solid particles. The resolution near 1 µm allowed analyzing large droplets and the impact of hydrodynamics but the role of local interaction important for small droplets could not be considered. The classical modeling methods (pore blocking and cake filtration, gel formation) didn't show reliable results for polydisperse deformable droplets [30]. The cleaning of the membrane fouled with oil is difficult because of the deformability of oil droplets and their propensity to form a continuous film [36][37] or to fill the pores and surface valleys [30].

In previous papers, conventional acid or basic solutions were tested to clean membranes fouled by lipids [38–40]. Trentin et al [40] studied the cleaning of nylon membranes used for oil/water premix emulsification. They demonstrated that a combination of ionic and nonionic surfactants, with NaOH at 50°C are the most efficient conditions. They demonstrated that a single cleaning step was not sufficient,

as described before by Silalahi et al [38] for the cleaning of ceramic membranes fouled by oily wastewater. Garmsiri et al. [39] showed that the binary or ternary solutions of anionic surfactants, EDTA and NaOH were the most efficient.

Zhu et al. [41] studied the filtration of emulsions in presence of NaCl and demonstrated that NaCl 10 mM reduced the interfacial tension of water/oil interface stabilized by anionic surfactants because it decreased the electrostatic repulsion between the charged heads of the surfactants. This was confirmed by Wu et al [42]. Kumar et al [43] also explained that this decrease in interfacial tension for NaCl Concentration between 17 mM and 100 mM leads to the formation of elongated worms like micelles with a smaller diameter. At higher NaCl concentration, the emulsion droplets tend to coalesce. The NaCl also affects the wetting of polysulfone ultrafiltration membrane [41] and the adsorption of surfactants at the solid or oil interface [42]. Moreover, Yan et al., 2020 [44], demonstrated that water containing low NaCl concentrations can be effectively used for the removal of oil trapped into a pore size capillary. The effect of salinity on the confined crude oil droplet was explained by two mechanisms: emulsification and water diffusion through the oil phase. The authors also showed that surface tension decreased with small salt concentrations, but it increased with high salt concentrations, making more efficient the remobilization of the entrapped oil at low NaCl concentrations.

Thus NaCl precleaning as described by Corbatón-Báguena [45] could help the destabilization of the lipid foulants. However, to our knowledge, NaCl solutions have not yet been considered for this purpose. The development of an innovative cleaning procedure, based on low cost and environmentally friendly solutions and limiting the use of chemicals that damage membranes, such as NaClO, could be of great interest, not only for microalgae fractionation processes but also for many other applications in oil and gas, pharmaceutical, food and beverage or in cosmetic industries [26].

The efficiency of NaCl precleaning for 0.1 µm polyethersulfone membranes fouled with a synthetic emulsion was first investigated. The impact of NaCl concentration and temperature on membrane fouling was evaluated by assessing the Hydraulic Cleaning Efficiency (HCE) of each cleaning step. Then, pristine, fouled and precleaned membranes were fully characterized to gain mechanistic understanding of the impact of NaCl on the membrane fouling. For this purpose, an innovative fouling characterization method based on electrokinetic measurements was implemented [46] and complemented by Scanning Electron Microscopy (SEM) coupled to Energy-Dispersive X-ray spectroscopy (EDX) measurements,

Fourier Transform InfraRed spectroscopy in Attenuated Total Reflection mode (ATR-FTIR) and Atomic Force Microscopy (AFM).

2 Theoretical part: definition of the Hydraulic Cleaning Efficiency (HCE)

According to the Darcy's law, the permeate flux through the membrane J (m s^{-1}) is proportional to the transmembrane pressure TMP (Pa), the permeate viscosity μ (Pa.s) and the resistance of the porous media to the permeation R (m^{-1}) according to Eq. (1).

$$J = \frac{TMP}{\mu \times R} \quad (1)$$

Based on the resistances-in-series model, after a water flush, the resistance to deionized water permeation R_h can be estimated as the sum of the clean membrane resistance R_m, the resistance of the physically reversible fouling R_φ, the resistance of the chemically reversible fouling R_χ, and the resistance of the irreversible fouling R_{irr} (Eq. (2)).

$$R_h = R_m + R_\varphi + R_\chi + R_{irr} \quad (2)$$

In this work, the physically reversible fouling corresponded to the fouling eliminated by water recirculation without and with pressure. The chemically reversible fouling was considered to be composed of three parts, each of which was eliminated by one of the following specific steps:

1- A precleaning step with NaCl
2- A basic commercial detergent cleaning
3- A cleaning polishing with NaClO

Thus, the resistance of the chemically reversible fouling was calculated as the sum of the three corresponding resistances:

$$R_\chi = R_{\chi\_NaCl} + R_{\chi\_det} + R_{\chi\_NaOCl} \quad (3)$$

The hydraulic cleaning efficiency HCE_i of each chemical step i was calculated with Eq (4) according to Corbatón-Báguena et al [47] using the measurement of water flux J_i at a chosen TMP and calculation of the remaining resistance R_i after each step: R_0 the resistance to water permeation after water precleaning (30°C), R_1 after NaCl precleaning, R_2 after the detergent cleaning and R_3 after NaClO cleaning polishing.

$$HCE_i = \frac{R_{i-1} - R_i}{R_0 - R_m} \quad (4)$$

For example, the hydraulic cleaning efficiency of the NaCl precleaning was determined as follows:

$$HCE_{NaCl} = HCE_1$$

$$= \frac{R_0 - R_1}{R_0 - R_m} = \frac{(R_m + R_{\chi_{NaCl}} + R_{\chi\_det} + R_{\chi_{NaOCl}} + R_{irr}) - (R_m + R_{\chi\_det} + R_{\chi_{NaOCl}} + R_{irr})}{R_{\chi_{NaCl}} + R_{\chi\_det} + R_{\chi_{NaOCl}} + R_{irr}}$$

$$HCE_{NaCl} = \frac{R_{\chi\_NaCl}}{R_{\chi\_NaCl} + R_{\chi\_det} + R_{\chi\_NaOCl} + R_{irr}} \quad (5)$$

3 Materials and methods

3.1 Experimental strategy

The experimental strategy developed was based on a two-phase approach (**figure** 1):

- the selection of an appropriate NaCl precleaning condition using HCE calculation,
- the analysis of the impact of NaCl precleaning by membrane fouling characterization.

Successive filtration/cleaning experiments were first carried out with the same membrane A (two membrane coupons in parallel, A1 and A2) to identify the optimal NaCl precleaning conditions (concentration and temperature). The efficiency of each combination (concentration, temperature) was evaluated by measuring the water permeability recovery and calculating the related HCE (Eq (4)). After each experiment, detergent cleaning and hypochlorite cleaning polishing steps were performed to recover comparable membrane water permeability and surface properties. The impact of NaCl precleaning on HCE was evaluated.

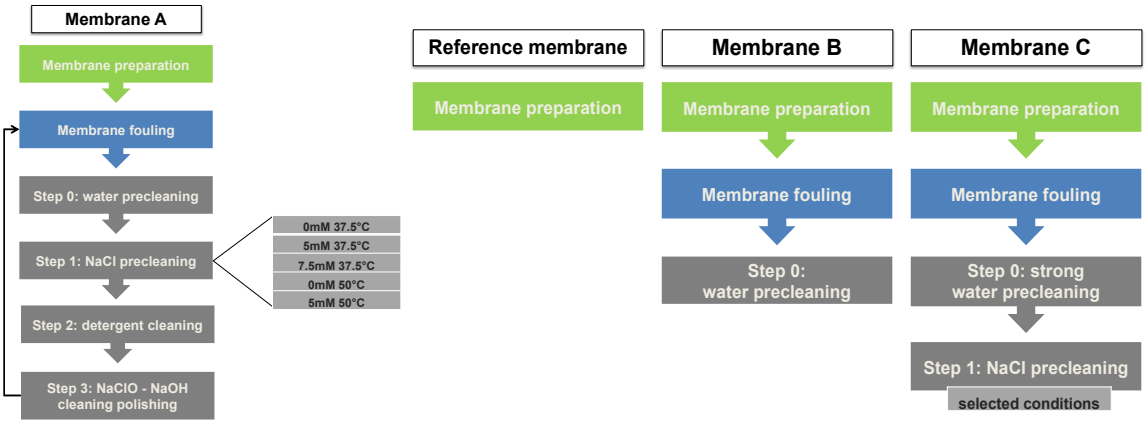

(i) (ii)

Figure 1: strategy followed in the study; (i) Identification of the appropriate NaCl precleaning conditions; (ii) characterization of the fouled and NaCl precleaned membranes to understand the impact of NaCl on fouling.

In a second stage, the impact of NaCl precleaning on fouling organization was investigated. For this purpose, new membrane coupons were conditioned in three different ways and characterized by SEM-EDX, FTIR-ATR, AFM and electrokinetic measurements:

- clean pristine membranes–referred to as 'Reference membrane'–
- membranes fouled and precleaned with water at 30 °C –referred to as 'membrane B'–,
- membranes fouled and precleaned using water and the appropriate NaCl conditions identified previously –referred to as 'membrane C'.

3.2 Ultrafiltration experiments

All fouling and cleaning experiments were performed using a cross-flow filtration pilot (see **Figure 2**) equipped with an ultrafiltration module (Rayflow X100, Orelis-Novasep, France) that can accommodate one or two membrane coupons in parallel, with a filtration area of 127 cm^2 each. Crossflow circulation of the feed was ensured by an eccentric rotor displacement pump, monitored and adjusted thanks to a flowmeter located on the recycling loop. In order to enhance the back-transport mechanisms near the membrane surface, a spacer of 1.05 mm (reference 46 mil) was used and the apparent crossflow velocity was set (see below). Permeation through the membrane was ensured by applying a constant

transmembrane pressure (TMP) adjusted by means of a back-pressure valve. The permeate flux was measured by collecting the permeate in a beaker placed on an electronic scale (model XL1200C, Precisa, Switzerland). Two pressure sensors placed at the module inlet and outlet on the retentate side allowed TMP monitoring and adjustment. A heat exchanger maintained the feed tank at constant and controlled temperature [48]. Each filtration experiment was performed in duplicate using two different membrane coupons. All results presented in this paper are the average values (RSD < 8%).

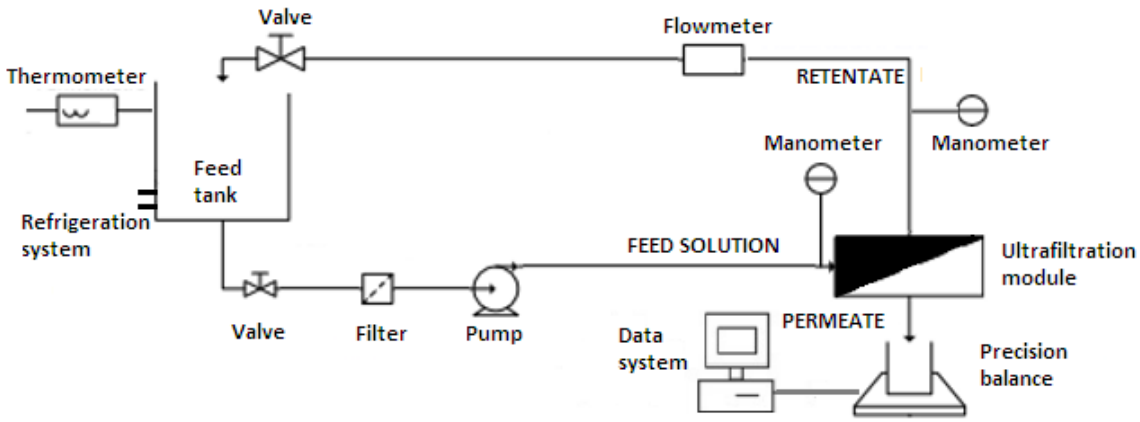

Figure 2: Schematic diagram of the ultrafiltration pilot.

3.3 Membrane material and preparation

Polyethersulfone (PES) microfiltration flat-sheet membranes with an average pore diameter of 0.1 µm (MFK618 Koch, USA) were used in this work. Before measurements, the membranes were first cleaned according to the following protocol: (i) filtration of 0.1% formulated alkaline detergent Ultrasil 115 solution at pH 11.4, 45 °C (Ecolab, France) (ii) filtration of a mixture of 0.1 $g.L^{-1}$ NaOH and 0.02 $g.L^{-1}$ NaClO (100 ppm) at pH 10.4, 30 °C. Both steps were performed without pressure for 20 minutes (apparent velocity in a free liquid channel: v_{app}: 0.4 $m.s^{-1}$) and under pressure (0.43 bar) for another 20 minutes (v_{app}: 0.8 $m.s^{-1}$). Between each cleaning step, the membranes were carefully rinsed using deionized (DI) water (30 °C) until the permeate reached a neutral pH. After cleaning, the membranes were compacted by carrying out DI water (30 °C) filtration at a constant TMP of 2 bar until a steady-state water flux was reached (± 5%). After compaction, the membranes were left in the pilot for overnight. The next day, water filtration was performed at the working pressure until a stable water flux was reached (see the example shown in Appendix).

3.4 Fouling experiments

Fouling experiments were further conducted using a 2% oil-in-water emulsion as feed solution. It was developed in a previous study [3] as a model system representative of the supernatant of a concentrated pretreated culture of *Parachlorella kessleri* microalgae, after bead milling and separation of the cell fragments by centrifugation. The aqueous phase had a pH of 7.4 and a conductivity of 790 µS cm^{-1}. The lipid phase consisted in a mixture of vegetable oils containing 70 wt % of neutral lipids and 30 wt % of apolar and negatively charged polar lipids at the pH under consideration [3,49].

Fouling experiments were conducted with 2 liters of emulsion, at a constant TMP of 0.43 bar, with an apparent crossflow velocity in a free liquid channel of v_{app}=0.8 $m.s^{-1}$ and at constant temperature near 30 °C. These operating conditions were maintained for 3 hours, under full recycling mode (permeate and retentate were systematically returned to the feed tank). It was previously shown by Clavijo Rivera et al [3] that the flux during the filtration of this emulsion was stable after 3 hours.

3.5 Membrane rinsing and cleaning

The identification of the appropriate NaCl cleaning conditions was done with membrane coupons A1 and A2 according to the following procedure. A water precleaning was first performed after the 3-hour fouling step (step 0). It consisted in a DI water flush (15 L at 30 °C) to remove the remaining emulsion. Next, DI water was recirculated into the pilot without pressure for 20 minutes (v_{app}: 0.4 $m.s^{-1}$), then under constant pressure of 0.43 bar for another 20 minutes (v_{app}: 0.8 $m.s^{-1}$) at 30 °C.

Once the water precleaning step was completed, the NaCl precleaning (step 1) was undertaken. Based on previous works [19–21], two NaCl concentrations (5 and 7.5 mM) were used at 37.5 °C. These low concentrations should both help diminish the oil/water interfacial tension and modify the wettability of the membrane as explained in literature [41–43][44]. These concentrations were selected because, as demonstrated by Manciu and Ruckenstein, 2003 [50] for concentrations lower than 7.5 mM, the surface tension of NaCl aqueous solutions is smaller than water surface tension. However, if concentration is higher than this value, the surface tension of the solution significantly increases with concentration, which negatively affects the cleaning efficiency. Then the impact of temperature was evaluated at 50 °C with the selected concentration (5 mM; see below). These conditions were compared to control experiments performed at the same temperatures but without NaCl (**Figure** 1) [47]. It can be mentioned that 50 °C is a usual temperature for PES membrane cleaning in industry and Kumar showed that this rise of temperature may destabilize emulsions [43]. Although a lower temperature could help reduce

energy consumption, at a temperature lower than 30 °C, some lipids could solidify and thus become difficult to be removed. For each condition, NaCl cleaning was performed at ambient pressure for 20 minutes (v_{app}: 0.4 $m.s^{-1}$) and under 0.43 bar for another 20 minutes (v_{app}: 0.8 $m.s^{-1}$). Between each experiment, the detergent and hypochlorite cleaning steps were performed (steps 2 and 3, respectively) to recover comparable water permeability and surface properties of coupons A1 and A2, following the protocol described for membrane preparation. The various steps are summarized in Appendix.

After each rinsing and cleaning step, DI water permeability measurements (30 °C) were performed to assess R_0, R_1, R_2 and R_3, which were further used to determine HCE by means of Eq (4) [47].

The water permeation measured before each experiment progressively increased from 104 to 215 L/h/m2/bar due to the unavoidable aging of the membrane material. These values were consistent with those described in the literature [51]. The modification of the intrinsic resistance of the membrane R_m was considered for each new experiment by measuring the new initial water flux.

For the fouling characterization (with and without NaCl precleaning), the membrane B was strongly rinsed with water (step 0) whereas the membrane C was strongly rinsed with water and then with NaCl solution (Steps 0 and 1).

3.6 Fouling characterization

The second part of this paper aimed to analyze the impact of NaCl precleaning on membrane fouling. For this purpose, an extensive characterization of the pristine membrane (reference membrane), the fouled membrane (membrane B) and the membrane precleaned with NaCl (membrane C) was undertaken.

3.6.1 SEM-EDX

Membrane samples were dried for several days (between 3 and 5 days) at 35–40°C and ambient pressure (until a constant sample mass was measured) before being characterized by scanning electron microscopy (SEM). All membranes were fixed on a SEM mount and sputtered with a 2–5 nm thick platinum layer (JEOL JUC5000) to render their surface conductive. Data acquisition was performed using the ZEISS Cross Beam 550 L SEM assisted by SmartSEM ZEISS software. Secondary electron (SE) SEM images were obtained using a relatively low-voltage value, 5 keV, of the primary electrons and ≈ 600 pA of beam current. Imaging was performed using three different detectors: a SESI detector (secondary electrons secondary ion detector) and an InLens (immersion lens) detector, both of which were used to

detect secondary electrons, as well as a BSD (backscattered detector) for detection of backscattered electrons, BSE. The InLens SE detector typically collects SEs with higher efficiency and thus provide images with higher contrast than the SESI detector [52,53]. These differences in electron energy collection were used to distinguish the presence of lipids on the membranes surface (see more detailed explanation in Appendix). Additionally, the BSD detector provided additional information from images with chemical contrast of the sample.

Energy-dispersive X-ray spectroscopy (EDX) analysis was performed using ULTIM MAX Large Area SDD Oxford energy-dispersive spectrometer attached to the ZEISS Cross Beam 550 L SEM and assisted by the AztecLive software. Membranes surface areas, where SE and BSE SEM image contrast was consistent with the presence or the absence of lipids, were analyzed by placing a focused electron beam at an incidence point and collecting X-rays emitted from the sample on an EDX spectrum. EDX analysis was performed on each area of interest (same incident point) using 4, 7 and 10 keV energies of the incident electron beam and ≈600 pA of current during 50 seconds of acquisition. Characteristic intensities were plotted using logarithmic scale after energy and intensities normalization, dividing them by the product of the beam current (in nA) and the acquisition time (in seconds) (0.6 nA*50s = 30).

3.6.2 ATR-FTIR

The ATR-FTIR spectra were recorded with a FT/IR 4100 Jasco spectrometer equipped with an ATR accessory (Miracle) having a ZnSe single reflection crystal with an incidence angle of 45°. Each spectrum was the accumulation of 128 scans with 2 cm^{-1} resolution in the 3700-600 cm^{-1} range, with the background recorded in ambient air. The data were then processed using the Spectra Manager software (5.0). Height measurements on the raw spectra were achieved after setting the baseline between 2240 and 2060 cm^{-1} (a region without any absorption bands). Membrane samples were carefully dried under dynamic vacuum at least three days before ATR-FTIR analyzes to remove adsorbed water and avoid the associated absorption band (large band around 3300 cm^{-1} and harmonic band at 1660 cm^{-1}). Three spectra were acquired for each membrane sample and the quantitative results are the average of these three measurements. Following the methodology proposed by Delaunay et al [54], the concentration of lipids deposited on the membrane was evaluated through calculation of the $\frac{h_{emulsion}}{h_{PES}}$ ratios, $h_{emulsion}$ being a band of high intensity typical of oil-in-water emulsion and h_{PES} being a band of high intensity typical of PES. The band at 1744 cm^{-1} (C=O stretching, fatty acid triglycerides or phospholipids

esters) was chosen for the emulsion, and the band at 1576 cm^{-1} (C=C) was chosen for PES membranes, both being of high intensity and without overlap with other bands.

3.6.3 AFM

The membrane roughness was analyzed by a MultiMode AFM with Nanoscope V controller and equipped with a 10 µm scanner from Digital Instruments (Veeco Metrology Group, Santa Barbara, CA, USA) in a tapping mode. A surface area of 5 µm × 5 µm of the membrane was chosen for the analysis. Three roughness parameters were studied:

(i) R_a, the arithmetic average of the roughness profile (µm)

$$R_a = \frac{1}{n}\sum_{i=1}^{n}|y_i| \quad (6)$$

(ii) R_q, the root mean square deviation of the assessed profile (µm)

$$R_q = \sqrt{\frac{1}{n}\sum_{i=1}^{n}(y_i - y_{avg})^2} \quad (7)$$

(iii) and R_z, the maximum height of the profile (µm)

$$R_z = max_i y_i + |min_i y_i| \quad (8)$$

3.6.4 Electrokinetic measurements

The electrokinetic measurements were performed with a Surpass electrokinetic analyzer (Anton Paar GmbH) equipped with an adjustable-gap cell requiring two membrane samples (each one 2 x 1 cm) [55]. The streaming current technique was used instead of streaming potential to avoid difficulties associated with the contribution of the membrane porous body to the cell electrical conductance [56]. Experiments were performed at T = 20 ± 2 °C with 500 mL of a 0.001 M KCl solution, the pH of which was adjusted with a 0.05 M HCl solution and kept constant within ± 0.05 throughout the course of the experiment. Prior to measurements, the solution was circulated through the channel for *ca.* 2 h to allow the sample equilibration. After equilibration, the streaming current was measured and recorded for increasing pressure differences (ΔP) up to 300 mbar. Measurements were repeated by progressively decreasing

the distance between the membrane samples (h_{ch}) from ~100 µm to ~40 µm by means of the micrometric screws of the adjustable-gap cell [46].

4 Results

Several cleaning conditions were first considered to evaluate the interest of NaCl precleaning. In the second part of this study, the impact of NaCl precleaning on the organization of membrane fouling by lipids was evaluated.

4.1 Identification of the appropriate NaCl precleaning conditions using HCE analysis

In the following paragraphs, the fouling experiments performed before the cleaning steps are presented. Then, the efficiency of NaCl precleaning was evaluated and the impact on the following steps (detergent cleaning and bleach cleaning polishing) was evaluated.

4.1.1 Fouling experiments

Figure 3 shows the evolution of flux as a function of time during the successive filtrations of emulsions using the membrane A (average flux values for coupons A1 and A2). Each curve corresponds to the fouling step of the membrane coupons, before the various precleaning and cleaning steps. The corresponding NaCl precleaning conditions are indicated in the legend.

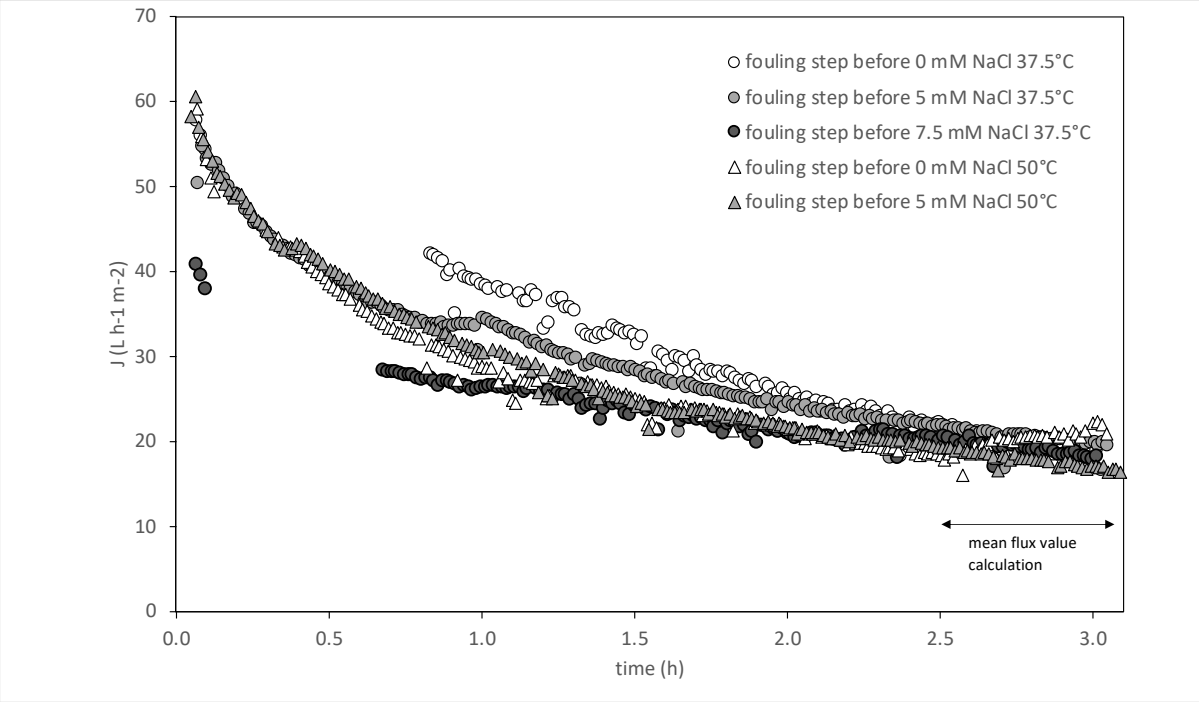

Figure 3: Permeate flux as a function of time during the filtration of emulsion using membrane A (average flux values for coupons A1 and A2).

All curves indicate a decrease in flux with time, which is typical of a progressive membrane fouling during the filtration of emulsion. For all experiments, the average final flux was calculated over the last 30 minutes of filtration. The final flux was between 17.5 and 20.4 $L.h^{-1}.m^{-2}$, with RSD ranging from 11 to 19%. These values are of the same order of magnitude as the fluxes observed during the filtration of supernatants from disrupted *Parachlorella kessleri* (PES MFK 618, KOCH, flux of 24 $L.h^{-1}.m^{-2}$ [57]) or from chlorella vulgaris (PES MFK 618, KOCH, flux of 7.8-13 $L.h^{-1}.m^{-2}$ [7]).

4.1.2 Cleaning experiments

Figure 4 presents the effect of NaCl precleaning, U115 detergent cleaning and NaClO-NaOH cleaning polishing on the water flux recovery after membrane fouling by the emulsion and water precleaning at 30 °C. The efficiency of each step is presented on the basis of HCE values calculated from Eq. (4).

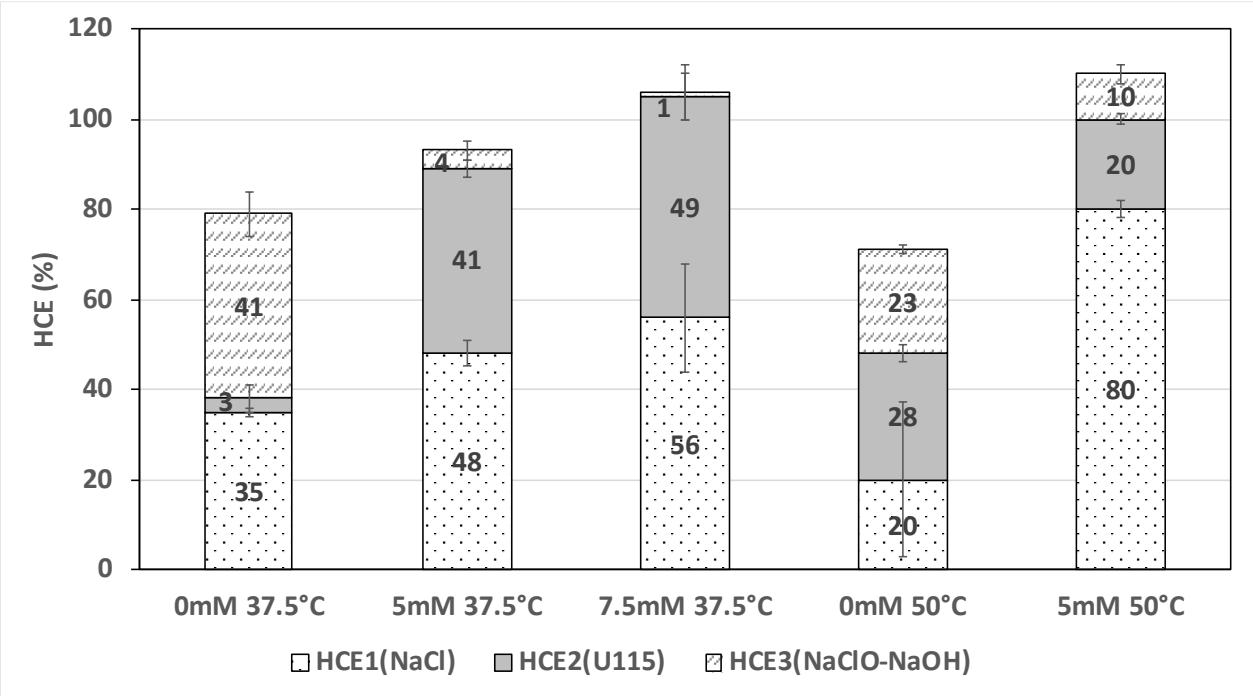

Figure 4 : Effect of NaCl concentration (0 mM (control), 5 mM or 7.5 mM) and temperature (37.5°C or 50°C) on the hydraulic cleaning efficiency (HCE) of NaCl precleaning (step 1), detergent U115 cleaning

(step 2) and NaClO-NaOH cleaning (step 3). Membranes were previously rinsed with water at 30°C in step 0.

Efficiency of the NaCl precleaning

At 37.5 °C, HCE_{NaCl} was found to increase with NaCl concentration, rising from 35% with DI water to 56% with 7.5 mM NaCl. However, although the presence of salt improved the hydraulic cleaning efficiency, no significant impact of the salt concentration between 5 mM and 7.5 mM on HCE_{NaCl} was found (48 ± 5% and 56 ± 12% for 5 mM and 7.5 mM, respectively).

The existence of an optimal NaCl concentration was already reported, by several authors, the value depending on the compounds/membranes considered [10,21,58]. Lee and Elimelech (2007) highlighted an optimal NaCl concentration of 50 mM for cleaning of reverse osmosis membrane fouled with alginate and calcium solutions above which the HCE remained constant [10]. They explained this finding by the fact that, above 50 mM, the physical conditions were not enough to ensure an effective mass transfer of the cleaning reaction products away from the membrane. Other authors reported that exceeding the optimal NaCl cleaning concentration might lead to a decrease in the cleaning efficiency [47,58]. Some authors claimed that it could be related to the impact of salt on the surface tension. When dealing with proteins, Tsumoto et al. demonstrated that, in the low salt concentration range, surface tension decreased as salt concentration increased. On the contrary, they showed that surface tension increased linearly with salt concentration for high salt concentrations [58]. They concluded that the removal of protein-based fouling compounds by solubilization was favored at low salt concentrations. In our case, i.e. lipid-based fouling, a decrease in the interfacial tension under the action of NaCl was discussed by several authors [41–43][44] for different lipid emulsions, stabilized by different amphiphilic compounds. It was shown that NaCl could lead to the emulsification of the oil remaining on the membrane surface [59,60]. Once stabilized, the oil droplets might become easier to remove by the back-transport mechanisms induced by the cross-flow velocity. Yan et al, 2020 probed that water containing low NaCl concentrations was effective to remove oil trapped into a pore size capillary because of emulsification and improved water diffusion through the oil phase. Thus the remobilization of the entrapped oil was more efficient at low NaCl concentrations [44]. However, once the NaCl concentration becomes high enough to stabilize all the oil droplets, an increase in NaCl concentration does not lead to a better cleaning efficiency. NaCl concentrations above 100 mM (not the case here) could even lead to a larger coalescence [43].

At 5 mM NaCl, increasing the solution temperature from 37.5 °C to 50 °C resulted in a much higher HCE (HCE_{NaCl} up to 80%), in agreement with what was reported in the literature [18–20,47]. Such an impact of the temperature could result from a decrease of the surface tension and thus from the enhancement of the emulsification phenomenon, despite the decrease in the continuous phase viscosity [21].

Impact of NaCl precleaning conditions on U115 detergent cleaning efficiency

Membrane precleaning with NaCl solutions at 37.5 °C had an impact on the cleaning step with U115. Indeed, HCE_{U115} was very low (3%) when the membrane was precleaned with DI water whereas HCE_{U115} increased up to 41 and 49% when salt precleaning was performed beforehand. The impact of 5 and 7.5 mM NaCl cleaning on HCE_{U115} was similar (41 and 49%, respectively). This finding confirmed that the concentration of 5 mM in NaCl was enough to destabilize fouling. The impact of the NaCl precleaning step on the U115 cleaning step might be related to the destabilization of the fouling layer under the action of salt, which allowed the U115 detergent to access the foulant still present on and/or inside the membrane.

The impact of the precleaning performed with the 5 mM NaCl solution at 50 °C on the U115 efficiency was similar to that of DI water at 50°C but it allowed to reach $HCE_{NaCl+U115}$ equal to 100% in only two steps (i.e. without further polishing with NaClO-NaOH). The effect of salt on U115 efficiency could not be highlighted here because the NaCl precleaning was very efficient.

Impact of NaCl precleaning conditions on NaClO-NaOH cleaning efficiency

At 37.5 °C and 50 °C, the usefulness of NaClO-NaOH cleaning to recover the membrane initial performances was demonstrated when no NaCl was used. The HCE after water precleaning and the detergent U115 cleaning step was not high enough and NaClO-NaOH polishing led to an increase in HCE of 23–42% depending on the temperature. In both cases, a total HCE lower than 80% was reached after all the cleaning steps. On the other hand, the positive effect of NaClO-NaOH was very limited when a NaCl precleaning was performed beforehand. Indeed, the total cleaning efficiency after NaCl precleaning and U115 cleaning reached 90–100%. At 7.5 mM and 37.5 °C and at 5 mM and 50 °C, the NaClO-NaOH cleaning step led to HCE>100%, thus indicating a membrane modification. Flux measurements suggested that the cleaning polishing with NaOCl-NaOH could be avoided as 100% HCE was already achieved after the first two steps.

To sum up, 5 mM NaCl at 50 °C appeared to be the most suited NaCl precleaning condition. In these conditions, HCE up to 80% was observed after NaCl precleaning. Moreover, the U115 detergent cleaning step made possible to remove the remaining fouling as it allowed to reach 100% HCE and the final NaClO-NaOH polishing step was not required (except for disinfection purposes). In the next part of this study, we focused on the understanding of the impact of such precleaning conditions (5 mM NaCl 50 °C) on fouling by lipids.

4.2 Impact of NaCl precleaning on membrane fouling

Membranes B and C were cleaned, compacted and fouled according to the procedures described in the Material and methods section.

After the filtration of the emulsion, the membrane B was carefully rinsed with DI water to remove the remaining emulsion and the physically reversible part of fouling. The same water precleaning was carried out with membrane C, followed by NaCl precleaning using 5 mM NaCl at 50 °C. Following this methodology, a HCE_{NaCl} of 70% was obtained for membrane C, which nearly recovered its initial DI water permeability. This HCE_{NaCl} was slightly lower than the one observed previously when cleaning membrane A with 5 mM NaCl 50 °C (80%) but remained very high. The difference observed between membranes A and C might originate from either heterogeneity between the membrane coupons or the fact that the membranes A and C had different filtration backgrounds and ageing.

Further to these experiments, each membrane was prepared in order to be characterized by SEM-EDX, ATR-FTIR, AFM and electrokinetic measurements.

4.2.1 Scanning electron microscopy and EDX analysis

Figure 5 (i) shows SEM images of the membranes surface of a reference membrane (membrane ref), a fouled and water precleaned membrane (membrane B) and a fouled, water precleaned and NaCl precleaned membrane (membrane C). Images were obtained using the Inlens SE detector at low magnification. The contrast of the InLens SE images was compared to SE images formed using the SESI detector and to BSE images using the BSD detector (images on membrane B at higher magnification, 'B high-mag'). As compared to the SESI images, the InLens SE detector provides higher-resolution and higher-contrast imaging of unstained samples [52] particularly at the low voltages and small working distances [53] used in this work (see Methods section for the experimental details).

Notably, dark spots are observed on the InLens SE images of the surface of the B and C membranes in (i). The same spots were not observed in the reference membrane and thus are consistent with the presence of lipids on the fouled membranes surfaces. Furthermore, these darker areas are evident using the BSD detector, as well (figure 5(i), B high-mag), but are absent in SESI images. Such contrast is consistent with the presence of deposits of material formed by light elements on the surface, such as fouling of lipids. Following this interpretation, the fouling was revealed as dark spots by the more sensitive InLens detector. We note that, consistently with the fact that the resolution and contrast of SESI images, in the experimental conditions used, are lower than those of InLens images, the fouling of the membrane at the surface is not as evident in the SESI images at low magnification (images not shown); it appears only at higher magnifications (see the SEM-SESI image of the B membrane at higher magnification in (i)). In the SESI image, a deposit appears as blurred areas of the image on an otherwise porous surface. Finally, the contrast of the InLens images is consistent with a fouling being present before and after NaCl precleaning, as a heterogeneous deposit, far from a homogeneous film. The SEM images did not allow us to draw conclusions on the evolution of the surface deposit after NaCl precleaning.

In order to study the chemical composition of the deposits and to obtain information not only from the membranes' surface but also from deeper inside the membranes, EDX analysis with tuned primary energies of the electron beam was performed.

Figure 5 (ii) presents EDX spectra performed on dark (solid lines) and bright (dotted lines) areas identified on InLens SE images of the fouled and water precleaned membrane (membrane B, top graphs and images) and fouled, water precleaned and NaCl precleaned membrane (membrane C, bottom graphs and images). Spectra were acquired using 4 keV (blue lines), 7 keV (green lines) and 10 keV (red lines). For this analysis, the electron beam was focused at an incident point on the membrane surface (signaled by an X in the region of analysis images at the insets) and the X-rays emitted were collected. The region of analysis images was obtained using the InLens SE detector. The spectra show carbon (CK line energy), oxygen (OK line energy), sulfur (SK line energy) and platinum (PtM line energy) characteristic intensities collected on the 0–90 eV energy range. We note that EDX is less effective on light elements, which can be detected as long as their concentration is relatively high and their intensities do not overlap with stronger peaks from other chemical species. Notably, phosphorus (P) is present in low concentrations in phospholipids, and fell below the technical sensitivity of our detector. The EDX analysis reveals that dark and bright areas on the surface of the B and C membranes have similar light element detection (Carbon, Oxygen and Sulphur peak). Those light elements are part of the

PES membrane. Lipids also contain C and O. In order to study local variations on the content of carbon (which can be directly linked to the presence of lipids) near the surface and at increasing depths inside the membranes, the relative intensities of the CK peak on the EDX spectra measured using 4 keV, 7 keV and 10 keV from bright and dark areas and for membranes B and C were compared among each other.

Figure 5 (ii) shows enlarged views of the 7.3 - 10.7 eV energy range including the characteristic intensity CK_{α} corresponding to the K line energy of the carbon for membrane B (top) and membrane C (bottom). The origin depth within the membranes of the X-rays analyzed by EDX is proportional to the energy of the incident electron beam (i.e. the use of higher keV would produce EDX spectra with X-rays arising mostly from areas deeper within the sample) [61][62]. Here we compared 4 KeV EDX spectra (with a higher contribution of X-rays from areas closer to the surface of the membranes) with 7 keV and 10 keV spectra, where information would arise from deeper areas inside the membranes.

Firstly, by comparing the intensity of the CK peaks of bright areas and of dark areas, Figure 5 (ii) indicates that less carbon signal is systematically detected in the bright areas. This is strictly true for all cases measured, with the exception of the area near the surface (4 KeV) on membrane B, where the CK line, on both dark and bright areas, appears relatively similar. The link between the lipid fouling and dark areas is thus reinforced by our finding of a higher presence of carbon in dark areas as compared to bright areas at several depths. Since the dotted CK peaks are systematically lower than the solid peaks, our observations, therefore, are consistent not only with the presence of a deposit, with a high carbon content, on the dark areas in the InLens SE images, but also with a C-rich material filling the pores inside the membrane and at several depths below those dark areas.

Furthermore, The CK peaks on membrane C display general lower intensities than on membrane B, especially for the beam energies 7 and 10 keV. Such a decrease of carbon detected after the NaCl cleaning is consistent with the cleaning efficiency. This is particularly true for the membrane bright areas showing a better effectiveness of the NaCl cleaning. Additionally, the more significant difference of carbon intensity signal at 10 keV than at 4 keV is coherent with a larger efficiency of the NaCl cleaning in depth.

Thus, the EDX analysis confirmed the presence of carbon-rich elements in the dark areas and permitted to highlight the NaCl cleaning efficiency on filtration membranes, particularly deeper in the porous media.

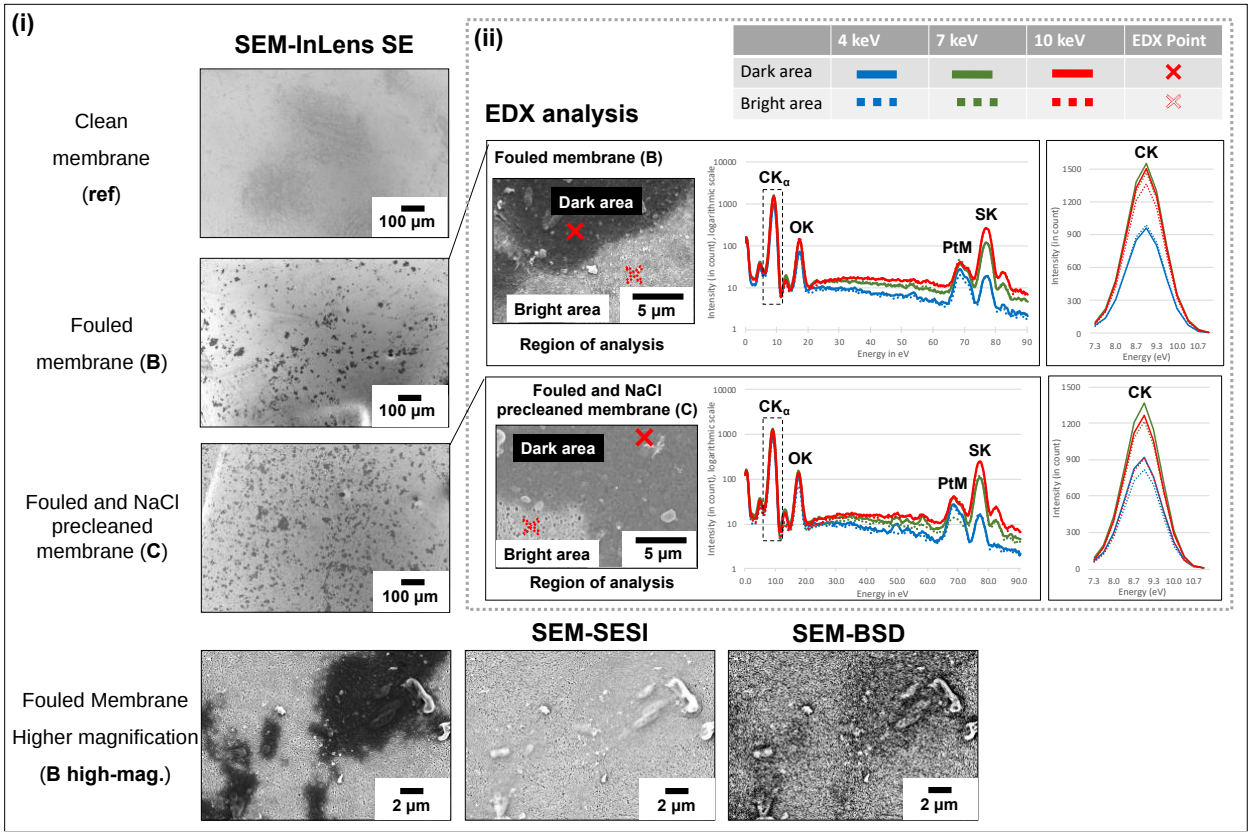

Figure 5: SEM observations and EDX analysis of clean (ref), fouled (B) and fouled and NaCl precleaned (C) membrane surfaces. 5 (i): Inlens SE images (5 keV beam energy, 600 pA beam current, 5 mm working distance) showing surface information are consistent with a heterogeneous distribution of lipid fouling at a specific point on the membranes' surface in B and C membranes. Images at higher magnification, M = 5 Kx, (B high-mag) show a comparison of the contrast observed from a closed-up area displaying the darker contrast consistent to the lipid fouling in SEM images with the InLens SE detector and two more detectors for SE (SESI) and BSE (BSD). 5 (ii): EDX analysis of dark (solid line) and bright (dotted line) areas by focusing the electron beam at an incident point (signaled by a X in the region of analysis pictures) and collecting the X-rays emitted. Red crosses show where the spectra were acquired at different incident electron beam energies. Spectra were acquired with 4, 7 and 10 keV of energy and ≈600 pA of current during 50 seconds of acquisition. Enlarged views of the carbon Kα intensity peaks indicated with dotted rectangles in the full EDX spectra are also shown.

4.2.2 ATR-FTIR

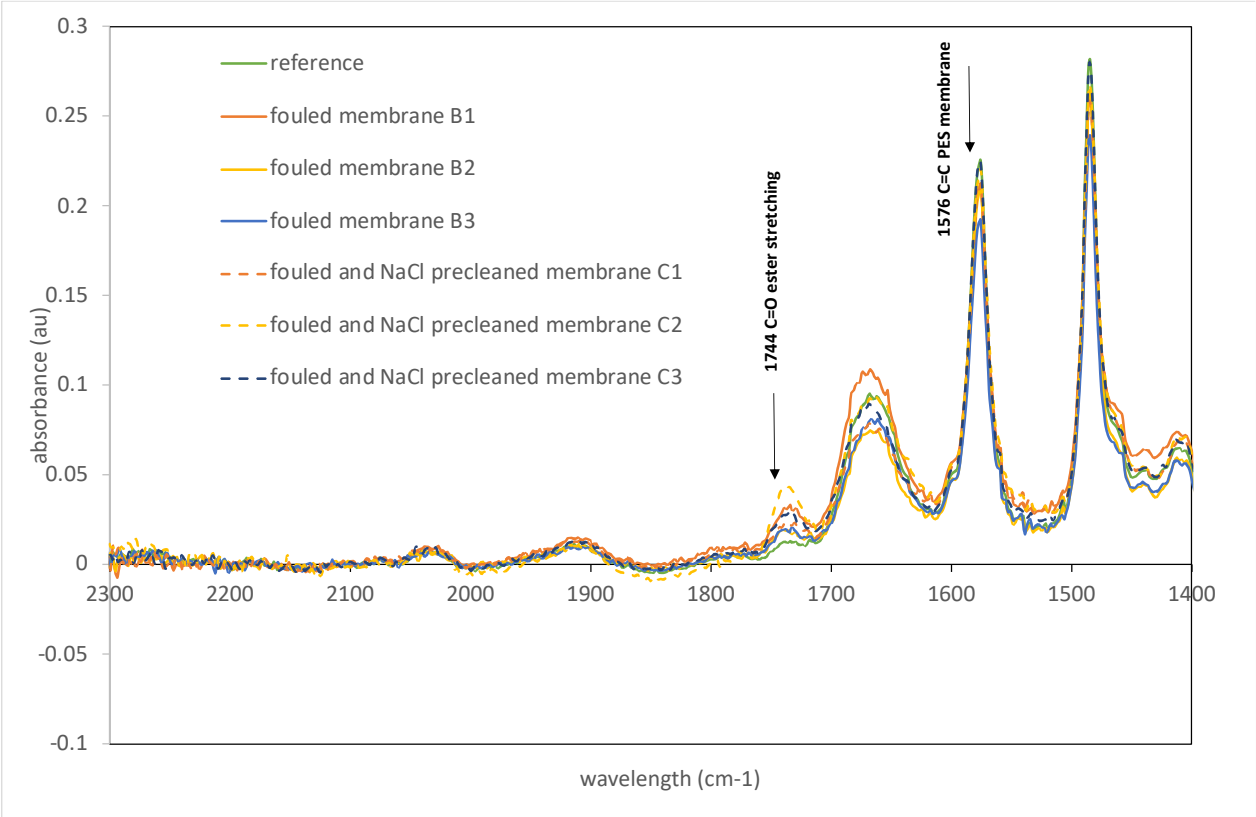

Figure 6: ATR-FTIR spectra of the clean membrane (reference), fouled membrane (B) and fouled and NaCl precleaned membrane (C).

Figure 6 presents the spectra of a pristine reference membrane, three different fouled membranes (B1, B2, B3) and three different NaCl precleaned membranes (C1, C2, C3). As expected, the reference membrane exhibited a low absorbance at the 1744 cm^{-1} band, with a $\frac{h_{1744}}{h_{1576}}$ ratio near 0.05. The presence of lipids, on both fouled and NaCl precleaned membranes, was validated by FTIR-ATR measurements, with ratios of 0.10 ± 0.02 and 0.12 ± 0.04, respectively. At first sight, no significant difference was noticed between the fouled and NaCl precleaned membranes. A more detailed analysis of the spectra, taking into account the lipids penetration into the membrane, will be developed in a subsequent work.

4.2.3 AFM

Figure 7 provides the three-dimensional AFM images of the various membranes.

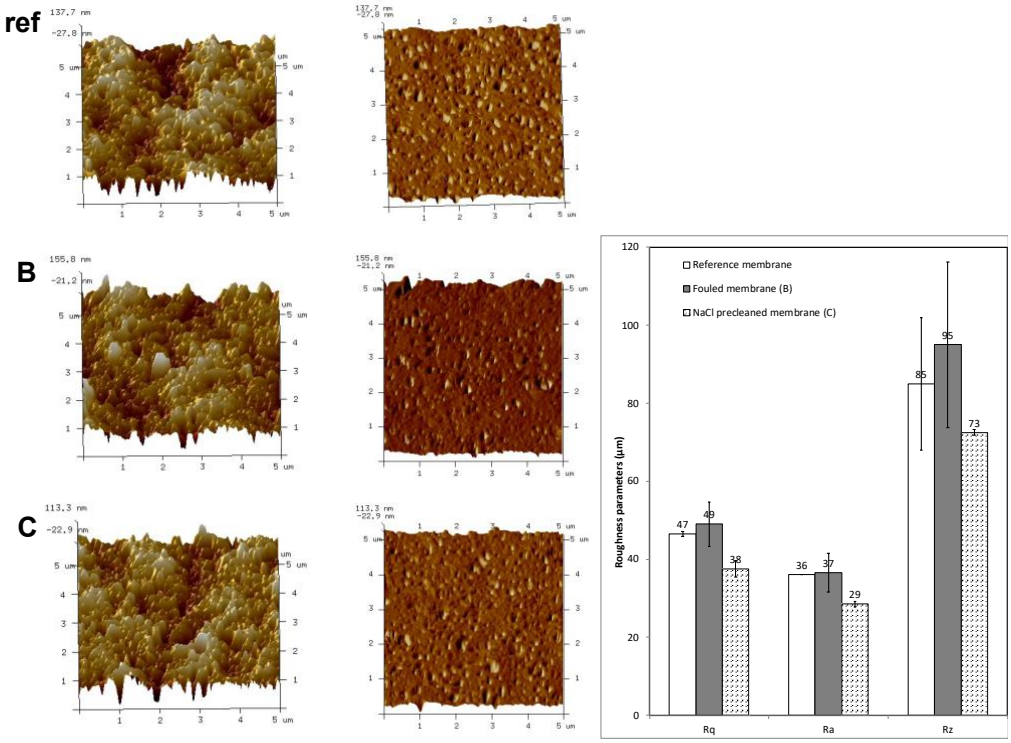

Figure 7 (i) Surface 3D AFM images, (ii) Roughness parameters (Rq, Ra, Rz), of a reference membrane (ref), a fouled membrane (B) and a precleaned membrane (C).

The brightest area corresponds to the highest points of the membrane surface while the darkest areas are associated with valleys or membrane pores. These images were numerically treated to extract roughness parameters, as shown in figure 7.

The roughness parameters observed for the fouled membranes were surprisingly similar to those of the reference membrane. Concerning the NaCl precleaned membrane, a significant decrease in R_q, R_a and R_z was highlighted. This decrease could be related to the formation of an oil deposit on the membrane surface. This phenomenon has already been observed during microfiltration of oily wastewater, but in the later stage of filtration and not after cleaning [63]. In our case, the change in ionic strength induced by NaCl might be responsible for the destabilization of oil fouling on the membrane surface, leading to a modification of the roughness.

4.2.4 Electrokinetic measurements

Tangential electrokinetic measurements are widely used to characterize fouling, as membrane charge is directly affected by the presence of fouling materials on its surface. However, in the case of porous materials such as micro- (MF) and ultrafiltration (UF) membranes, it has been shown that a part of the streaming current is likely to flow through the membrane porosity. Such a parasitic phenomenon has been known as electrokinetic leakage. In such a case, the measured current can be expressed by Eq. (9):

$$I_s^{tot} = I_s^{ch} + 2I_s^{pore} = -\left(\frac{Wh_{ch}\varepsilon_0\varepsilon_r\Delta P}{\eta L}\zeta_{surf} + \frac{2Wh_{mb}^{eff}\varepsilon_0\varepsilon_r\Delta P}{\eta L}\zeta_{pore}\right) \quad (9)$$

with I_s^{tot} the total streaming current (i.e. the experimentally measured current), I_s^{pore} the electrokinetic leakage occurring within a single membrane (two membrane samples separated by a distance h_{ch} are used in tangential electrokinetic measurements), I_s^{ch} the streaming current flowing through the channel formed by the two membrane surfaces, W and L the width and length of the samples, respectively, h_{mb}^{eff} the effective height where the electrokinetic leakage takes place in a single membrane (it includes the membrane thickness, porosity and tortuosity), ζ_{surf} and ζ_{pore} the zeta potential of the membrane surface and inside the membrane porosity, respectively, ε_0 the vacuum permittivity, ε_r and η the dielectric constant and the dynamic viscosity of the electrolyte solution respectively, and ΔP the pressure difference applied between the channel ends.

As shown by Rouquié *et al.* (2020), accounting for the electrokinetic leakage phenomenon can bring useful information about the presence of fouling material inside the membrane porosity. For this purpose, streaming current measurements performed at various channel heights (h_{ch}) can be carried out, to access the following information [46]:

- Real ζ_{surf} (from the slope of $I_s^{tot}/\Delta P$ vs. h_{ch})
- Total electrokinetic leakage (from the y-intercept of $I_s^{tot}/\Delta P$ vs. h_{ch})

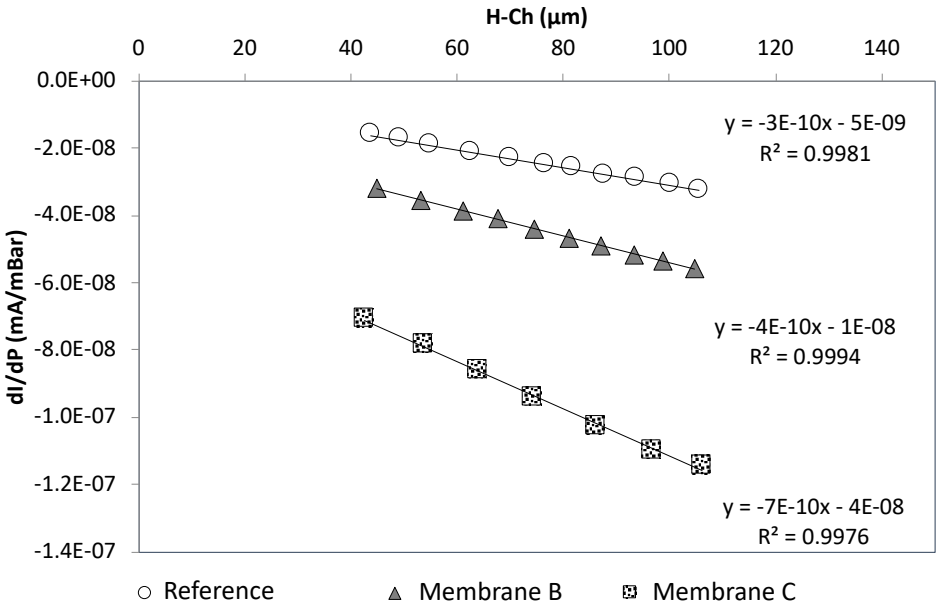

figure 8: Streaming current coefficient versus channel height (h-Ch) measured for pristine reference membrane (white circle), fouled membrane (B, gray triangle) and precleaned membrane (C, dot squares). Experiments were performed in a 0.001 M KCl solution at pH 5.00±0.05.

Figure 8 presents the streaming current coefficient versus channel height for a Reference membrane, a fouled membrane B and a NaCl precleaned membrane C.

From these measurements and Eq. (9), the surface zeta potential of the various membranes was calculated and results are collected in Table 1.

Table 1: Zeta potential of membrane surface

Sample	Surface zeta potential (mV)
Reference membrane	- 6.8 ± 0.1
membrane B	- 12.3 ± 2.2
membrane C	- 19.3 ± 2.1

The surface zeta potential of the pristine PES was quite low (-6.8 mV) [46]. When the membrane was fouled (membrane B), an increase of zeta potential in absolute value was observed (-12.3 mV), which

resulted from the greater negative charge of emulsion droplets accumulated on the membrane surface (−25.7 ± 1.1 mV).

An even more negative surface zeta potential (-19.3 mV) was observed after membrane cleaning by NaCl (membrane C) with a value closer to the emulsion charge. Despite water flux recovery induced by NaCl cleaning, it seems that more fouling material appeared on the membrane surface.

The magnitude of the electrokinetic leakage phenomenon depends on the following parameters:

- Membrane structure (pore size, porosity and pore tortuosity) and steric hindrance related to the presence of fouling inside the membrane
- Membrane and fouling charge
- Hydrophilicity/hydrophobicity of the membrane and fouling, which affects pore invasion by the electrolyte solution during electrokinetic measurements.

As shown in **figure** 8, the electrokinetic leakage is found greater for both the fouled (-10^{-8} mA.mbar^{-1}) and cleaned (-4.10^{-8} mA.mbar^{-1}) membranes compared with the pristine one (-5.10^{-9} mA.mbar^{-1}). This is related to the presence of charged foulant inside the membrane porous structures. Interestingly, the electrokinetic leakage is even higher after NaCl precleaning the membrane (the membranes were rinsed with deionized water before measurements to get rid of NaCl residues; see the materials and methods section). This result can be understood by considering that when the fouling material is more charged than the pristine membrane, there is an interplay between charge and steric-hindrance effects. The small amount of charged fouling material inside the membrane is likely to increase the electrokinetic leakage. However, beyond a threshold amount of fouling material, steric hindrance becomes the dominant effect and the electrokinetic leakage is expected to decrease as pressure-driven transport of ions in the pore-filling solution is more and more hindered (especially with hydrophobic lipid foulants). As a result, the electrokinetic leakage is expected to pass through a maximum as a function of the amount of charged fouling material inside the membrane structure. Results shown in **figure** 8 can then be explained by the positive impact of NaCl cleaning on internal fouling. By partially removing internal fouling, the NaCl cleaning step led to an increase in the electrokinetic leakage through the PES membrane. The more negative surface zeta potential obtained after NaCl precleaning (**Table** 1) might then be explained by fouling material dislodging from inside the pores to the membrane surface. This is consistent with the decrease of carbon content, more important in depth than on the surface shown by SEM-EDX analysis. It is also in agreement with the lower roughness of the NaCl precleaned membrane where gelled patches could be present. The electrokinetic leakage results also suggest that internal

fouling was not fully eliminated by the NaCl precleaning step as the electrokinetic leakage with the cleaned membrane was found to be different from that of the pristine membrane.

4.3 Discussion

All the results of HCE measurements and characterization methods can be gathered to build hypotheses on the fouling of the PES MFK618 membrane by a lipid emulsion (see figure 9), and the impact of the NaCl precleaning.

During the filtration of the emulsion, lipid droplets accumulated in both the membrane pores and onto the membrane surface. Water precleaning allowed the removal of a part of the physically reversible surface fouling. The remaining fouling on the surface of membrane B was observed by SEM as a non-regular deposit. An impact on the surface zeta potential was observed, but the fouling was not of sufficient magnitude to modify the surface roughness. The porous media fouled with lipids was more polar than the PES, leading to a slight increase of the electronic leakage. The NaCl precleaning led to the migration of a substantial part of the lipids from the pores to the surface of membrane C. This induced a rise of the water flux (increase in HCE after NaCl precleaning), the surface zeta potential and the electronic leakage inside pores. Some polar lipids were still present in the membrane, but the streaming current inside pores was much less hindered, due to fouling dislodgment from the pores to the membrane surface. The roughness was modified, maybe by the filling of valleys. The total amount of lipids on and in the membrane did not change; thus, no difference was highlighted by ATR-FTIR. In SEM-EDX, the drop of the carbon intensity after NaCl precleaning was more important in depth than on the surface. The difference between the results from ATR-FTIR (no elimination of lipids) and SEM-EDX (a loss of carbon after NaCl precleaning) could be due either to the impact of sample preparation before SEM on the lipid deposit at the membrane surface, or to the lack of ATR-FTIR sensitivity. After detergent cleaning, the majority of the lipids were removed and a very high HCE was reached compared with cleaning without NaCl. The bleach polishing led to a rise of the water flux, but the removal of lipids or the membrane modification could not be differentiated. These hypotheses will require subsequent works to be fully validated.

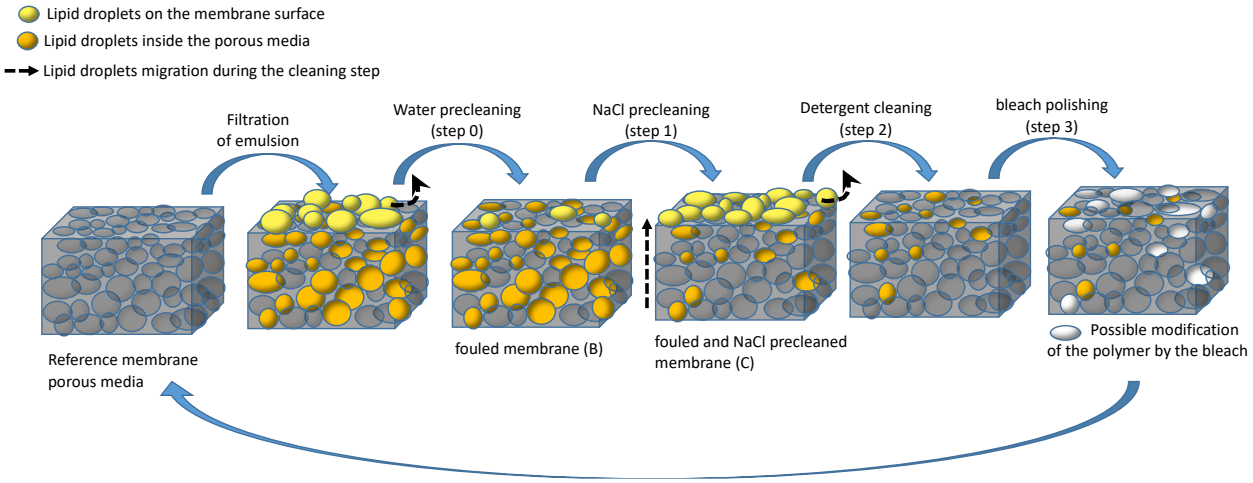

683

684 **Figure 9: graphical illustration of the membrane fouling by an emulsion and the impact of the**
685 **successive cleaning steps.**

686

687 ## 5 Conclusion

688 In this work, it was demonstrated that NaCl precleaning was efficient to strongly improve the cleaning
689 by a conventional detergent of a PES lipid-fouled membrane. Using appropriate NaCl concentration and
690 temperature (5 mM NaCl at 50 °C), the hydraulic cleaning efficiency of the NaCl precleaning and the
691 following detergent cleaning was considerably enhanced and allowed to recover the initial water flux
692 without the use of the NaClO polishing. This last step could then be reduced to disinfection. The use of
693 SEM-EDX, AFM, ATR-FTIR and electrokinetic measurements allowed demonstrating that fouling was
694 present on the surface as well as in the membrane pores and that it was irregularly organized in regions
695 containing larger and lower amounts of lipids. However, NaCl precleaning enabled a significant decrease
696 of the internal fouling by displacing lipids from the pores to the membrane surface and thus facilitating
697 the detergent cleaning step. In subsequent works, the efficiency of this cleaning procedure will be
698 assessed with complex mixtures containing lipids and proteins, such as microalgae extracts.

699

700

701 ## Acknowledgements and funding sources

This work was supported by the Challenge Food For Tomorrow/Cap Aliment, Pays de la Loire, France (project 3MFOODGY) and the SEM-EDX part by the NExT initiative through national funding by the French National Research Agency (ANR) under the Programme d'investissements d'Avenir (with reference ANR-16-IDEX-0007, project e-BRIDGE). The e-BRIDGE project also receives financial support from the Pays de la Loire and Nantes Métropole.

6 References

[1] R. Sathasivam, R. Radhakrishnan, A. Hashem, E.F. Abd_Allah, Microalgae metabolites: A rich source for food and medicine, Saudi Journal of Biological Sciences. 26 (2019) 709–722. https://doi.org/10.1016/j.sjbs.2017.11.003.

[2] P. Bernardo, A. Iulianelli, F. Macedonio, E. Drioli, Membrane technologies for space engineering, Journal of Membrane Science. 626 (2021) 119177. https://doi.org/10.1016/j.memsci.2021.119177.

[3] E. Clavijo Rivera, L. Villafaña-López, S. Liu, R. Vinoth Kumar, M. Viau, P. Bourseau, C. Monteux, M. Frappart, E. Couallier, Cross-flow filtration for the recovery of lipids from microalgae aqueous extracts: Membrane selection and performances, Process Biochemistry. 89 (2020) 199–207. https://doi.org/10.1016/j.procbio.2019.10.016.

[4] E. Lorente, M. Haponska, E. Clavero, C. Torras, J. Salvadó, Microalgae fractionation using steam explosion, dynamic and tangential cross-flow membrane filtration, Bioresource Technology. 237 (2017) 3–10. https://doi.org/10.1016/j.biortech.2017.03.129.

[5] C. Safi, G. Olivieri, R.P. Campos, N. Engelen-Smit, W.J. Mulder, L.A.M. van den Broek, L. Sijtsma, Biorefinery of microalgal soluble proteins by sequential processing and membrane filtration, Bioresource Technology. 225 (2017) 151–158. https://doi.org/10.1016/j.biortech.2016.11.068.

[6] A.-V. Ursu, A. Marcati, T. Sayd, V. Sante-Lhoutellier, G. Djelveh, P. Michaud, Extraction, fractionation and functional properties of proteins from the microalgae Chlorella vulgaris, Bioresource Technology. 157 (2014) 134–139. https://doi.org/10.1016/j.biortech.2014.01.071.

[7] S. Liu (a), I. Gifuni, H. Méar, M. Frappart, E. Couallier*, Recovery of soluble proteins from Chlorella vulgaris by bead-milling and microfiltration: Impact of the concentration and the physicochemical conditions during the cell disruption on the whole process., Process Biochemistry. (2021) accepted.

[8] M.L. Gerardo, D.L. Oatley-Radcliffe, R.W. Lovitt, Integration of membrane technology in microalgae biorefineries, Journal of Membrane Science. 464 (2014) 86–99. https://doi.org/10.1016/j.memsci.2014.04.010.

[9] J. Masojídek, G. Torzillo, Mass Cultivation of Freshwater Microalgae☆, in: Reference Module in Earth Systems and Environmental Sciences, Elsevier, 2014. https://doi.org/10.1016/B978-0-12-

409548-9.09373-8.

[10] S. Lee, M. Elimelech, Salt cleaning of organic-fouled reverse osmosis membranes, Water Research. 41 (2007) 1134–1142. https://doi.org/10.1016/j.watres.2006.11.043.

[11] C. Regula, E. Carretier, Y. Wyart, G. Gésan-Guiziou, A. Vincent, D. Boudot, P. Moulin, Chemical cleaning/disinfection and ageing of organic UF membranes: A review, Water Research. 56 (2014) 325–365. https://doi.org/10.1016/j.watres.2014.02.050.

[12] J. Ding, S. Wang, P. Xie, Y. Zou, Y. Wan, Y. Chen, M.R. Wiesner, Chemical cleaning of algae-fouled ultrafiltration (UF) membrane by sodium hypochlorite (NaClO): Characterization of membrane and formation of halogenated by-products, Journal of Membrane Science. 598 (2020) 117662. https://doi.org/10.1016/j.memsci.2019.117662.

[13] H. Liang, W. Gong, J. Chen, G. Li, Cleaning of fouled ultrafiltration (UF) membrane by algae during reservoir water treatment, Desalination. 220 (2008) 267–272. https://doi.org/10.1016/j.desal.2007.01.033.

[14] A.L. Ahmad, N.H. Mat Yasin, C.J.C. Derek, J.K. Lim, Chemical cleaning of a cross-flow microfiltration membrane fouled by microalgal biomass, Journal of the Taiwan Institute of Chemical Engineers. 45 (2014) 233–241. https://doi.org/10.1016/j.jtice.2013.06.018.

[15] Z. Wang, J. Ding, P. Xie, Y. Chen, Y. Wan, S. Wang, Formation of halogenated by-products during chemical cleaning of humic acid-fouled UF membrane by sodium hypochlorite solution, Chemical Engineering Journal. 332 (2018) 76–84. https://doi.org/10.1016/j.cej.2017.09.053.

[16] Y. Zhang, J. Tian, H. Liang, J. Nan, Z. Chen, G. Li, Chemical cleaning of fouled PVC membrane during ultrafiltration of algal-rich water, Journal of Environmental Sciences. 23 (2011) 529–536. https://doi.org/10.1016/S1001-0742(10)60444-5.

[17] Y. Hanafi, P. Loulergue, S. Ababou-Girard, C. Meriadec, M. Rabiller-Baudry, K. Baddari, A. Szymczyk, Electrokinetic analysis of PES/PVP membranes aged by sodium hypochlorite solutions at different pH, Journal of Membrane Science. 501 (2016) 24–32. https://doi.org/10.1016/j.memsci.2015.11.041.

[18] Z. Wang, Y. Li, P. Song, X. Wang, NaCl cleaning of 0.1μm polyvinylidene fluoride (PVDF) membrane fouled with humic acid (HA), Chemical Engineering Research and Design. 132 (2018) 325–337. https://doi.org/10.1016/j.cherd.2018.01.009.

[19] M.-J. Corbatón-Báguena, S. Álvarez-Blanco, M.-C. Vincent-Vela, Cleaning of ultrafiltration membranes fouled with BSA by means of saline solutions, Separation and Purification Technology. 125 (2014) 1–10. https://doi.org/10.1016/j.seppur.2014.01.035.

[20] M.-J. Corbatón-Báguena, A. Gugliuzza, A. Cassano, R. Mazzei, L. Giorno, Destabilization and removal of immobilized enzymes adsorbed onto polyethersulfone ultrafiltration membranes by salt solutions, Journal of Membrane Science. 486 (2015) 207–214. https://doi.org/10.1016/j.memsci.2015.03.061.

[21] M.-J. Corbatón-Báguena, S. Álvarez-Blanco, M.-C. Vincent-Vela, Salt cleaning of ultrafiltration membranes fouled by whey model solutions, Separation and Purification Technology. 132 (2014) 226–233. https://doi.org/10.1016/j.seppur.2014.05.029.

[22] H. Chang, F. Qu, B. Liu, H. Yu, K. Li, S. Shao, G. Li, H. Liang, Hydraulic irreversibility of ultrafiltration membrane fouling by humic acid: Effects of membrane properties and backwash water composition, Journal of Membrane Science. 493 (2015) 723–733. https://doi.org/10.1016/j.memsci.2015.07.001.

[23] H. Chang, H. Liang, F. Qu, S. Shao, H. Yu, B. Liu, W. Gao, G. Li, Role of backwash water composition in alleviating ultrafiltration membrane fouling by sodium alginate and the effectiveness of salt backwashing, Journal of Membrane Science. 499 (2016) 429–441. https://doi.org/10.1016/j.memsci.2015.10.062.

[24] E. Clavijo Rivera, V. Montalescot, M. Viau, D. Drouin, P. Bourseau, M. Frappart, C. Monteux, E. Couallier*, Mechanical cell disruption of Parachlorella kessleri microalgae: Impact on lipid fraction composition, Bioresour Technol. 256 (2018) 77–85. https://doi.org/10.1016/j.biortech.2018.01.148.

[25] L. Villafaña-López, E. Clavijo, S. Liu, E. Couallier, M. Frappart, Shear-enhanced membrane filtration of model and real microalgae extracts for lipids recovery in biorefinery context, Bioresource Technology. (2019) 121539. https://doi.org/10.1016/j.biortech.2019.121539.

[26] B. Chakrabarty, A.K. Ghoshal, M.K. Purkait, Cross-flow ultrafiltration of stable oil-in-water emulsion using polysulfone membranes, Chemical Engineering Journal. 165 (2010) 447–456. https://doi.org/10.1016/j.cej.2010.09.031.

[27] J. Saadati, M. Pakizeh, Separation of oil/water emulsion using a new PSf/pebax/F-MWCNT nanocomposite membrane, Journal of the Taiwan Institute of Chemical Engineers. 71 (2017) 265–276. https://doi.org/10.1016/j.jtice.2016.12.024.

[28] A. Salama, Investigation of the problem of filtration of oily-water systems using rotating membranes: A multicontinuum study, Colloids and Surfaces A: Physicochemical and Engineering Aspects. 541 (2018) 175–187. https://doi.org/10.1016/j.colsurfa.2018.01.015.

[29] A. Salama, Modeling of flux decline behavior during the filtration of oily-water systems using porous membranes: Effect of pinning of nonpermeating oil droplets, Separation and Purification Technology. 207 (2018) 240–254. https://doi.org/10.1016/j.seppur.2018.06.043.

[30] E. Tummons, Q. Han, H.J. Tanudjaja, C.A. Hejase, J.W. Chew, V.V. Tarabara, Membrane fouling by emulsified oil: A review, Separation and Purification Technology. 248 (2020) 116919. https://doi.org/10.1016/j.seppur.2020.116919.

[31] P. Loulergue, M. Weckert, B. Reboul, C. Cabassud, W. Uhl, C. Guigui, Mechanisms of action of particles used for fouling mitigation in membrane bioreactors, Water Research. 66 (2014) 40–52. https://doi.org/10.1016/j.watres.2014.07.035.

[32] H.J. Tanudjaja, V.V. Tarabara, A.G. Fane, J.W. Chew, Effect of cross-flow velocity, oil concentration and salinity on the critical flux of an oil-in-water emulsion in microfiltration, Journal of Membrane Science. 530 (2017) 11–19. https://doi.org/10.1016/j.memsci.2017.02.011.

[33] J. Tian, T.A. Trinh, M.N. Kalyan, J.S. Ho, J.W. Chew, In-situ monitoring of oil emulsion fouling in ultrafiltration via electrical impedance spectroscopy (EIS): Influence of surfactant, Journal of Membrane Science. 616 (2020) 118527. https://doi.org/10.1016/j.memsci.2020.118527.

[34] F. Doudiès, M. Loginov, N. Hengl, M. Karrouch, N. Leconte, F. Garnier-Lambrouin, J. Pérez, F. Pignon, G. Gésan-Guiziou, Build-up and relaxation of membrane fouling deposits produced during crossflow ultrafiltration of casein micelle dispersions at 12 °C and 42 °C probed by in situ SAXS, Journal of Membrane Science. 618 (2021) 118700. https://doi.org/10.1016/j.memsci.2020.118700.

[35] H.J. Tanudjaja, J.W. Chew, Critical flux and fouling mechanism in cross flow microfiltration of oil emulsion: Effect of viscosity and bidispersity, Separation and Purification Technology. 212 (2019) 684–691. https://doi.org/10.1016/j.seppur.2018.11.083.

[36] L. Zhu, M. Chen, Y. Dong, C.Y. Tang, A. Huang, L. Li, A low-cost mullite-titania composite ceramic hollow fiber microfiltration membrane for highly efficient separation of oil-in-water emulsion, Water Research. 90 (2016) 277–285. https://doi.org/10.1016/j.watres.2015.12.035.

[37] H.J. Tanudjaja, C.A. Hejase, V.V. Tarabara, A.G. Fane, J.W. Chew, Membrane-based

825 separation for oily wastewater: A practical perspective, Water Research. 156 (2019) 347–365.
826 https://doi.org/10.1016/j.watres.2019.03.021.

827 [38] S.H.D. Silalahi, T. Leiknes, Cleaning strategies in ceramic microfiltration membranes fouled by
828 oil and particulate matter in produced water, Desalination. 236 (2009) 160–169.
829 https://doi.org/10.1016/j.desal.2007.10.063.

830 [39] E. Garmsiri, Y. Rasouli, M. Abbasi, A.A. Izadpanah, Chemical cleaning of mullite ceramic
831 microfiltration membranes which are fouled during oily wastewater treatment, Journal of Water Process
832 Engineering. 19 (2017) 81–95. https://doi.org/10.1016/j.jwpe.2017.07.012.

833 [40] A. Trentin, C. Güell, T. Gelaw, S. de Lamo, M. Ferrando, Cleaning protocols for organic
834 microfiltration membranes used in premix membrane emulsification, Separation and Purification
835 Technology. 88 (2012) 70–78. https://doi.org/10.1016/j.seppur.2011.12.003.

836 [41] X. Zhu, A. Dudchenko, X. Gu, D. Jassby, Surfactant-stabilized oil separation from water using
837 ultrafiltration and nanofiltration, Journal of Membrane Science. 529 (2017) 159–169.
838 https://doi.org/10.1016/j.memsci.2017.02.004.

839 [42] J. Wu, P. Mei, J. Wu, J.-W. Fu, L. Cheng, L. Lai, Surface properties and microemulsion of
840 anionic/nonionic mixtures based on sulfonate Gemini surfactant in the presence of NaCl, Journal of
841 Molecular Liquids. 317 (2020) 113907. https://doi.org/10.1016/j.molliq.2020.113907.

842 [43] N. Kumar, S. Ali, A. Kumar, A. Mandal, Design and formulation of surfactant stabilized O/W
843 emulsion for application in enhanced oil recovery: effect of pH, salinity and temperature, Oil Gas Sci.
844 Technol. – Rev. IFP Energies Nouvelles. 75 (2020) 72. https://doi.org/10.2516/ogst/2020066.

845 [44] L. Yan, H. Aslannejad, S.M. Hassanizadeh, A. Raoof, Impact of water salinity differential on a
846 crude oil droplet constrained in a capillary: Pore-scale mechanisms, Fuel. 274 (2020) 117798.
847 https://doi.org/10.1016/j.fuel.2020.117798.

848 [45] M.J. Corbatón-Báguena, S. Álvarez-Blanco, M.C. Vincent-Vela, J. Lora-García, Utilization of
849 NaCl solutions to clean ultrafiltration membranes fouled by whey protein concentrates, Separation and
850 Purification Technology. 150 (2015) 95–101.

851 [46] C. Rouquié, S. Liu, M. Rabiller-Baudry, A. Riaublanc, M. Frappart, E. Couallier, A. Szymczyk,
852 Electrokinetic leakage as a tool to probe internal fouling in MF and UF membranes, Journal of
853 Membrane Science. 599 (2020) 117707. https://doi.org/10.1016/j.memsci.2019.117707.

[47] M.-J. Corbatón-Báguena, S. Álvarez-Blanco, M.-C. Vincent-Vela, J. Lora-García, Utilization of NaCl solutions to clean ultrafiltration membranes fouled by whey protein concentrates, Separation and Purification Technology. 150 (2015) 95–101. https://doi.org/10.1016/j.seppur.2015.06.039.

[48] C. Carbonell-Alcaina, S. Álvarez-Blanco, M.A. Bes-Piá, J.A. Mendoza-Roca, L. Pastor-Alcañiz, Ultrafiltration of residual fermentation brines from the production of table olives at different operating conditions, Journal of Cleaner Production. 189 (2018) 662–672. https://doi.org/10.1016/j.jclepro.2018.04.127.

[49] L. Villafaña-López, E. Clavijo Rivera, S. Liu, E. Couallier, M. Frappart, Shear-enhanced membrane filtration of model and real microalgae extracts for lipids recovery in biorefinery context, Bioresource Technology. 288 (2019) 121539. https://doi.org/10.1016/j.biortech.2019.121539.

[50] M. Manciu, E. Ruckenstein, Specific ion effects via ion hydration: I. Surface tension, Advances in Colloid and Interface Science. 105 (2003) 63–101. https://doi.org/10.1016/S0001-8686(03)00018-6.

[51] S. Habibi, M. Rabiller-Baudry, F. Lopes, F. Bellet, B. Goyeau, M. Rakib, E. Couallier, New insights into the structure of membrane fouling by biomolecules using comparison with isotherms and ATR-FTIR local quantification, Environmental Technology. (2020) 1–18. https://doi.org/10.1080/09593330.2020.1783370.

[52] B.J. Griffin, A comparison of conventional Everhart-Thornley style and in-lens secondary electron detectors-a further variable in scanning electron microscopy, Scanning. 33 (2011) 162–173. https://doi.org/10.1002/sca.20255.

[53] K. Kumagai, T. Sekiguchi, Sharing of secondary electrons by in-lens and out-lens detector in low-voltage scanning electron microscope equipped with immersion lens, Ultramicroscopy. 109 (2009) 368–372. https://doi.org/10.1016/j.ultramic.2009.01.005.

[54] D. Delaunay, M. Rabiller-Baudry, J.M. Gozálvez-Zafrilla, B. Balannec, M. Frappart, L. Paugam, Mapping of protein fouling by FTIR-ATR as experimental tool to study membrane fouling and fluid velocity profile in various geometries and validation by CFD simulation, Chemical Engineering and Processing: Process Intensification. 47 (2008) 1106–1117. https://doi.org/10.1016/j.cep.2007.12.008.

[55] A. Szymczyk, Y.I. Dirir, M. Picot, I. Nicolas, F. Barrière, Advanced electrokinetic characterization of composite porous membranes, Journal of Membrane Science. 429 (2013) 44–51. https://doi.org/10.1016/j.memsci.2012.11.076.

[56] P. Fievet, M. Sbaï, A. Szymczyk, C. Magnenet, C. Labbez, A. Vidonne, A New Tangential Streaming Potential Setup for the Electrokinetic Characterization of Tubular Membranes, Separation Science and Technology. 39 (2004) 2931–2949. https://doi.org/10.1081/SS-200028652.

[57] S. Liu, Fractionnement de biomolécules issues de microalgues par filtration membranaire : Impact du milieu complexe sur les performances du procédé / Fractionation of biomolecules from microalgae by membrane filtration: impact of the complex medium on the process performances., PhD thesis, Nantes University, 2021.

[58] K. Tsumoto, D. Ejima, A.M. Senczuk, Y. Kita, T. Arakawa, Effects of salts on protein–surface interactions: applications for column chromatography, Journal of Pharmaceutical Sciences. 96 (2007) 1677–1690. https://doi.org/10.1002/jps.20821.

[59] F. Yang, S. Liu, J. Xu, Q. Lan, F. Wei, D. Sun, Pickering emulsions stabilized solely by layered double hydroxides particles: The effect of salt on emulsion formation and stability, Journal of Colloid and Interface Science. 302 (2006) 159–169. https://doi.org/10.1016/j.jcis.2006.06.015.

[60] X. Cai, X. Du, G. Zhu, C. Cao, Induction effect of NaCl on the formation and stability of emulsions stabilized by carboxymethyl starch/xanthan gum combinations, Food Hydrocolloids. 105 (2020) 105776. https://doi.org/10.1016/j.foodhyd.2020.105776.

[61] M. Green, V.E. Cosslett, The Efficiency of Production of Characteristic X-radiation in Thick Targets of a Pure Element, Proceedings of the Physical Society. 78 (1961) 1206–1214. https://doi.org/10.1088/0370-1328/78/6/315.

[62] M. Essani, E. Brackx, E. Excoffier, A method for the correction of size effects in microparticles using a peak-to-background approach in electron-probe microanalysis, Spectrochimica Acta Part B: Atomic Spectroscopy. 169 (2020) 105880. https://doi.org/10.1016/j.sab.2020.105880.

[63] X. Xu, J. Li, N. Xu, Y. Hou, J. Lin, Visualization of fouling and diffusion behaviors during hollow fiber microfiltration of oily wastewater by ultrasonic reflectometry and wavelet analysis, Journal of Membrane Science. 341 (2009) 195–202. https://doi.org/10.1016/j.memsci.2009.06.009.

7 Appendix

Appendix A

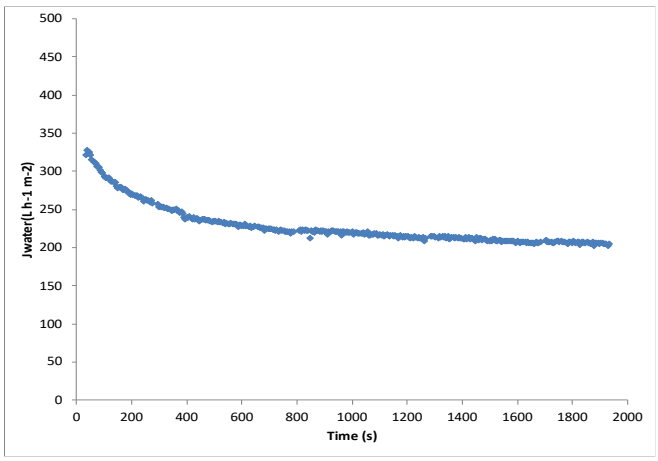

Figure A1: Time evolution of water flux (TMP = 0.43bar and T = 30°C) before fouling and cleaning steps.

Appendix B

The cleaning strategy, i.e. the operating conditions applied for each cleaning step, are gathered and summarized in the Table B1.

Table B1: Operating conditions associated with each cleaning step.

Feed	Temperature (°C)	Filtration time (minutes)	TMP (bar)	Cross-flow velocity ($m.s^{-1}$)
0. Water precleaning				
DI water flushing				
DI water	30	20	/	0.4
DI water recirculating				
DI water	30	20	/	0.4
DI water	30	20	0.43	0.8
1. NaCl precleaning				
NaCl (0 / 5 / 7.5 mM)	37.5 / 50	20	/	0.4
NaCl (0 / 5 / 7.5 mM)	37.5 / 50	20	0.43	0.8
2. U115 cleaning				
U115 (0.1%)	45	20	/	0.4
U115 (0.1%)	45	20	0.43	0.8
3. NaClO - NaOH cleaning				
NaOH (0.1 $g.L^{-1}$) **NaClO** (100 ppm)	30	20	/	0.4
NaOH (0.1 $g.L^{-1}$) **NaClO** (100 ppm)	30	20	0.43	0.8

924

925 Appendix C

926 SEM-EDX

927 The InLens SE detector was located in the SEM column above the specimen, while the SESI detector was
928 located in the SEM chamber (at an angle from the optical axis of the microscope). At the low voltage (5
929 KeV) and a small working distance (WD = 5mm) used, the InLens SE detector typically collected SEs with
930 higher efficiency and thus provided images with higher contrast than the SESI detector

931 . In other words, in the experimental conditions used here, with relatively low-voltage, no stage tilt and
932 a working distance of WD = 5 mm between the lower pole piece in SEM system and the sample surface,
933 electrons with a broad range of energies were collected by the InLens SE detector. In comparison, the
934 SESI detector collected mostly highly energized electrons. These differences in electron energy
935 collection were used to distinguish the presence of lipids on the membranes surface. Additionally, the
936 BSD detector provided additional information from images with chemical contrast of the sample.

937 The EDX technique presents a sensibility to material density and thus, to empty spaces such as pores.
938 The EDX signals detected arise from the X-rays interaction volume within the membrane. Since
939 microfiltration membranes are porous media, presenting larger pore size with increasing depth, this
940 may have consequences for the quality of the analyses.

941